Journal of Marine Research, 60, 779–803, 2002

Potential vorticity "crises", adverse pressure gradients, and western boundary current separation

by Andrew E. Kiss[1]

ABSTRACT

The vorticity dynamics involved in western boundary current separation are investigated in a depth-averaged barotropic single-gyre circulation forced by a spatially uniform wind stress curl in a circular basin on a beta-plane. The mechanism of separation is of interest in this simple model because it lacks most of the features (such as a change in sign of the wind stress curl, collision with another western boundary current, outcropping of isopycnals or an abrupt change in bottom topography or boundary shape) often associated with boundary current separation.

It has been suggested that a "crisis" due to insufficient recovery of potential vorticity Q in the outer boundary current outflow can result in separation. However, the numerical results and analysis presented here demonstrate that under no-slip boundary conditions the opposite "crisis" occurs in the viscous sublayer of the western boundary current, where fluid columns acquire more Q than they lost in the interior. The outflow must, therefore, adopt a configuration which dissipates this excess Q before fluid elements return to the interior flow. It is shown that under strongly nonlinear conditions sufficient viscous dissipation of Q can only be obtained when the outflow separates from the boundary; this flow structure is also associated with an "adverse" ageostrophic pressure gradient along the boundary. Under the free-slip boundary condition the cyclonic sublayer is absent, so there is no "crisis" of excess Q and the separation behavior is markedly different.

1. Introduction

Identifying the dynamics responsible for western boundary current separation has been a long-standing puzzle in geophysical fluid dynamics, which has attracted significant attention because inaccurate prediction of the separation site has been a persistent problem in ocean general circulation models (McWilliams, 1996; Dengg *et al.,* 1996). Among the factors which have been shown to influence separation in particular models are a change in sign of the wind stress curl (Munk, 1950),[2] a collision with another western boundary current (Cessi, 1991; Agra and Nof, 1993), a region of "adverse" longshore pressure gradient (Haidvogel *et al.,* 1992; Baines and Hughes, 1996), the requirement of potential vorticity balance (Verron and Le Provost, 1991), outcropping of isopycnals (Parsons, 1969; Veronis, 1973; Ou and de Ruijter, 1986) or a change in bottom topography or

1. Research School of Earth Sciences, Australian National University, Canberra, ACT 0200, Australia. ***email: andy@rses.anu.edu.au***

2. This is actually an artefact of the zonally uniform wind stress curl (Rhines and Schopp, 1991).

boundary shape (Pedlosky, 1965; Greenspan, 1963; Spitz and Nof, 1991; Dengg, 1993; Özgökmen *et al.,* 1997). The separation behavior is typically strongly dependent on the type of boundary condition used, occurring earlier and more abruptly with no-slip than with free-slip conditions (Blandford, 1971; Moro, 1988; Haidvogel *et al.,* 1992; Dengg, 1993; Verron and Jo, 1994).

This paper presents an investigation of the dynamics which produce western boundary current (WBC) separation in a simple homogeneous model of a single gyre driven by a spatially uniform wind stress curl in a circular basin. This is one of the simplest mid-latitude gyre models in which separation has been observed (Beardsley, 1969; Becker and Page, 1990; Griffiths and Kiss, 1999), despite the absence of most of the features associated with separation in other models. The mechanism responsible for the apparently unprovoked separation in this "lowest common denominator" model is therefore of interest, as it could also operate in more dynamically complex models.

The pivotal question addressed here is why the flow in a nonlinear Munk-type model is not a straightforward modification of the linear solution, but involves qualitatively new features such as separation and recirculation. This is a particularly difficult inertial-viscous boundary layer problem which has received considerable attention (see Pedlosky, 1996, for a comprehensive overview). The fundamental issue is that the potential vorticity lost[3] in the Sverdrup interior must be recovered on every streamline in the western boundary current return flow. When the inertial boundary-layer scale significantly exceeds the viscous sublayer width, only a small proportion of the streamlines will pass through the viscous region in which the recovery takes place. As a result, fluid in the outer WBC will have insufficient potential vorticity recovery. It has been shown (Kamenkovich, 1966; Ierley and Ruehr, 1986; Ierley, 1987) that the boundary-layer approximation breaks down under surprisingly weak nonlinearity when the boundary current outflow must be matched to a sufficiently rapid eastward Sverdrup flow. This breakdown has been related to the formation of a compact recirculation gyre in the northwest which is driven by (and serves to dissipate) the anomalous potential vorticity of the outer western boundary current (Cessi *et al.,* 1987; Ierley and Young, 1988; Cessi, 1990). The recirculation is thus the flow's response to a "crisis" of insufficient potential vorticity recovery in the outer western boundary current.

It has been known since the pioneering numerical experiments by Blandford (1971) that the choice of boundary conditions can strongly influence WBC separation behavior. Blandford used a barotropic single-gyre model with lateral and bottom friction. Under strong forcing and a free-slip boundary condition the WBC extends right along the northern boundary and rejoins the interior from the northeast as a relatively broad stream that encloses a weak recirculation spanning the width of the basin. Changing the boundary condition to no-slip yields a very different flow, in which the recirculation retreats to the

3. To avoid unnecessary complexity an anticyclonic wind stress will be assumed throughout this paper; analogous arguments apply under cyclonic forcing.

northwest corner, and the WBC separates as a concentrated jet after flowing only a short way along the northern boundary. There is a viscous sublayer embedded within the broader inertial WBC under either boundary condition, and we would expect a similar "crisis" of insufficient potential vorticity recovery in both cases, which would therefore drive a similar type of recirculation. The marked difference suggests that WBC separation, and therefore the zonal extent of the recirculation, is strongly influenced by the presence of a cyclonic region against the boundary as a consequence of the no-slip condition.

In contrast to the outer WBC, relatively little attention has been paid to the potential vorticity dynamics which pertain to the sublayer itself, where it has been assumed that ample viscous torque precludes any potential vorticity "crises." It is the purpose of this paper to demonstrate that under the no-slip condition the potential vorticity recovery in the cyclonic part of the sublayer can exceed that required to match the interior flow, necessitating a region of potential vorticity *loss* in the sublayer outflow. This is a "crisis" of the opposite kind to that previously discussed, and its resolution involves changes to the potential vorticity structure which act to steer the outer western boundary current offshore to produce a separated jet. The jet in turn restricts the size of the recirculation driven by the potential vorticity anomaly in the outer WBC. This "crisis" does not occur under the free-slip condition with a straight or concave boundary (because the entire boundary current is anticyclonic), explaining the different separation behavior in that case.

This paper is arranged as follows. In Section 2 the model equations and the numerical methods employed to solve them are described. In Section 3 the model results and analysis are presented, first with an overview of the phenomena in question (Section 3a), then focusing on the potential vorticity dynamics (Section 3b) and the way in which the potential vorticity "crisis" is resolved (Section 3c); this expands and generalizes the arguments put forward by Kiss (2001). The role of the pressure gradient is described in Section 3d. Discussion and conclusions are given in Section 4.

2. Model equations

We consider the wind-driven circulation of a homogeneous fluid in a circular basin of diameter L and uniform depth H, damped by Laplacian lateral viscosity and Rayleigh bottom friction. Taking the β-plane and rigid-lid approximations and averaging over the depth we obtain the nondimensional momentum equation

$$\delta_I^2\left[\frac{\partial \mathbf{u}}{\partial t} + (\mathbf{u}\cdot\nabla)\mathbf{u}\right] + (f_0 + y)\hat{\mathbf{k}}\times\mathbf{u} = -\nabla p + \tau - \delta_S\mathbf{u} + \delta_M^3\nabla^2\mathbf{u}, \tag{2.1}$$

where $\mathbf{u} = \hat{\mathbf{k}}\times\nabla\psi$ is the depth-averaged horizontal velocity (nondivergent due to mass conservation), ψ is the streamfunction, f_0 is the Coriolis parameter at the origin, x and y are the eastward and northward coordinates, p is the pressure and the surface stress is modelled as a body force τ. The length scale chosen for the nondimensionalisation is the basin diameter L. We use an advective timescale L/U, where the velocity scale $U = \tau_0/(\rho\beta LH)$

is obtained from the Sverdrup balance in the interior (here τ_0 is a representative dimensional surface stress magnitude and ρ is the fluid density). Thus $f_0 = f_0^*/(\beta L)$, where $f^* = f_0^* + \beta L y$ is the dimensional Coriolis parameter. The pressure is scaled by $\rho U \beta L^2$. The scaling in (2.1) is similar to that of Ierley and Sheremet (1995) and Pedlosky (1987, Section 5.4), except for the use of an advective timescale.

The form of the solution is determined by the three dimensionless parameters δ_S, δ_M and δ_I, where

$$\delta_S = L^{-1}\left(\frac{A_V f_0^*}{2\beta^2 H^2}\right)^{1/2} \tag{2.2}$$

is the Stommel (1948) western boundary-layer width (indicating the importance of bottom friction),

$$\delta_M = L^{-1}\left(\frac{A_H}{\beta}\right)^{1/3} \tag{2.3}$$

is the Munk (1950) western boundary-layer width (indicating the strength of lateral viscosity), and

$$\delta_I = L^{-1}\left(\frac{U}{\beta}\right)^{1/2} \tag{2.4}$$

is the inertial boundary current width, which indicates the importance of advection. Here A_V and A_H are the coefficients of vertical and horizontal turbulent diffusion.

The vertical component of the curl of (2.1) yields the governing nondimensional vorticity equation

$$\frac{\partial Q}{\partial t} + J(\psi, Q) = W - \delta_S \zeta + \delta_M^3 \nabla^2 \zeta, \tag{2.5}$$

where

$$\zeta = \nabla^2 \psi \tag{2.6}$$

is the relative vorticity, $W = \hat{\mathbf{k}} \cdot \nabla \times \tau$, $Q = \delta_I^2 \zeta + y$ is the potential vorticity (so $J(\psi, Q) = \delta_I^2 J(\psi, \zeta) + \partial\psi/\partial x$ combines the vorticity advection and β terms), and $J(a, b) \equiv (\partial a/\partial x)(\partial b/\partial y) - (\partial a/\partial y)(\partial b/\partial x)$ is the Jacobian. We consider the simplest possible wind forcing, $W = -1$ (i.e. a spatially uniform anticyclonic wind stress curl). The vorticity equation (2.5) was solved numerically, using boundary conditions of zero mass flux

$$\psi = 0 \quad \text{at } r = \tfrac{1}{2} \tag{2.7}$$

and either no-slip

$$\frac{\partial \psi}{\partial r} = 0 \quad \text{at } r = \frac{1}{2} \tag{2.8}$$

or zero-vorticity

$$\zeta = 0 \quad \text{at } r = \tfrac{1}{2}, \tag{2.9}$$

where r is the radial coordinate. The zero-vorticity boundary condition does not imply zero stress, since the stress is due only to the shear, and not the component of the vorticity due to the solid-body rotation involved in following the curved boundary. A zero-vorticity condition is used here as a simple way to eliminate the cyclonic layer found next to the wall under no-slip conditions, in order to illustrate the effect this has on WBC separation. A free-slip (i.e. no-stress) condition requires weak anticyclonic vorticity at the boundary in this geometry, and the absence of the cyclonic layer would yield a flow nearly identical to that with a zero-vorticity condition. With the parameters used here the boundary stress under the zero-vorticity condition is about 100 times smaller than with no-slip.

The numerical model was based on a code developed by Page (1982), which was modified to solve (2.5) using conservative second-order finite differences on a polar grid. The alternating-direction implicit method was used for temporal advancement of ζ by Eq. (2.5), and the Poisson equation (2.6) was solved for ψ using a direct method based on a fast Fourier transform in θ. An in-timestep iteration served to converge ζ at the boundary to a value which was consistent with the no-slip boundary condition (when this was applied), and also to allow relaxation of the advective term which couples ψ and ζ. The code is described in detail in Kiss (2000). Most of the numerical results reported here were obtained using a uniform grid with 160 radial and 512 azimuthal points; since we investigate flows with δ_S, $\delta_M > 10^{-2}$, these radial length scales are resolved with more than three radial grid points. The integration was continued until the flow had adjusted to its asymptotic state (a steady circulation for most of the results reported here). A few runs at higher spatial and temporal resolution were used to confirm that the processes were sufficiently well-resolved.

Convergence could be very slow when bottom friction was absent (i.e. $\delta_S = 0$), due to the very slow decay of large-scale basin modes. In some cases an acceleration technique described by Berloff and Meacham (1997) was employed in order to filter out these oscillations and reach the steady state more rapidly. This involved repeatedly "collapsing" the streamfunction and vorticity fields onto their average over an oscillation period as the time integration proceeded; each "collapse" could reduce the oscillation amplitude by an order of magnitude or more. The stability of the steady state could be assessed by observing whether the remaining infinitesimal oscillation tended to grow or decay when the flow was allowed to evolve freely.

The vorticity equation (2.5) with boundary conditions (2.7) and (2.8) is almost identical to that investigated by Griffiths and Kiss (1999) in their study of the "sliced cylinder" laboratory model of wind-driven circulation (in which β is simulated by a depth gradient),

the only difference being a slight north-south variation in β, W and δ_S due to the relative depth variation. They used a different scaling in their formulation, in which the dimensionless parameters are the Rossby number $Ro = 2(L/H)^2\delta_M^3\delta_I^2/\delta_S^3$, the Ekman number $E = 4(L/H)^4\delta_M^6/\delta_S^2$ (a factor of 2 appears since Ekman layers occur on both the top and bottom boundaries), the bottom slope $s = 2(L/H)\delta_M^3/\delta_S^2$ and the aspect ratio $L/H = 7.84$; their results can be compared with those presented here by using these conversion formulae. Similar models with a circular geometry have also been studied by Pedlosky and Greenspan (1967), Beardsley (1969, 1972, 1973), Beardsley and Robbins (1975), Becker and Page (1990) and Briggs (1980).

3. Results and analysis

We will concentrate on the evolution of the steady flow as δ_I is increased, while (δ_S, δ_M) are held fixed at either (1.43×10^{-2}, 1.09×10^{-2}) or (0, 2.00×10^{-2}). The runs with no-slip boundary conditions and (δ_S, δ_M) = (1.43×10^{-2}, 1.09×10^{-2}) are dynamically almost identical to the sliced cylinder experiments of Griffiths and Kiss (1999) with $E = 1.25 \times 10^{-4}$, $s = 0.1$ and $L/H = 7.84$. The numerical results are used to provide illustrative examples of the generic qualitative changes which occur as the western boundary current outflow becomes more nonlinear. Thus the actual values chosen for δ_S and δ_M are not critical, and the main requirement is that the boundary currents are narrow relative to the basin width, as in the oceans.

a. Overview

Anticyclonic wind stress drives a slow southward Sverdrup flow in the interior which is returned in a rapid western boundary current (WBC). Beardsley (1969) showed that in the linear limit ($\delta_I = 0$) the character of the WBC depends on the relative size of δ_M and δ_S. When $\delta_M \gg \delta_S$ we have a Munk (1950)-type boundary current, in which lateral viscosity balances the β term and the meridional velocity has an oscillatory decay in x. When $\delta_M \ll \delta_S$ most of the boundary current is anticyclonic, in a Stommel (1948) balance between bottom friction and β, and the velocity profile decays monotonically in x. However for all $\delta_M \neq 0$ there must also be a thin sublayer (of thickness $(\delta_M^3/\delta_S)^{1/2}$) in which the tangential velocity is adjusted to match the boundary condition (2.8) or (2.9) via a balance between lateral viscosity and bottom friction. As δ_M approaches and then exceeds δ_S in magnitude the boundary layer changes from Stommel- to Munk-type. The oscillatory velocity profile appears first at $y = 0$, when $\delta_M = 4^{1/3}\delta_S/3$, then rapidly spreads north and south as δ_M increases. Under near-linear conditions $\psi = O(1)$ at its maximum, located on the line $y = 0$ where the meridional velocity changes sign at the outer edge of the WBC. In the Munk limit ($\delta_M \gg \delta_S$) the peak velocity is $O(\delta_M^{-1})$ and the vorticity in both the anticyclonic outer WBC and the cyclonic region near a no-slip boundary is $O(\delta_M^{-2})$. In the Stommel limit ($\delta_M \ll \delta_S$) the peak velocity is $O(\delta_S^{-1})$ and the vorticity is $O(\delta_S^{-2})$ in the anticyclonic region and $O(\delta_S^{-1/2}\delta_M^{-3/2})$ in the cyclonic sublayer under no-slip conditions.

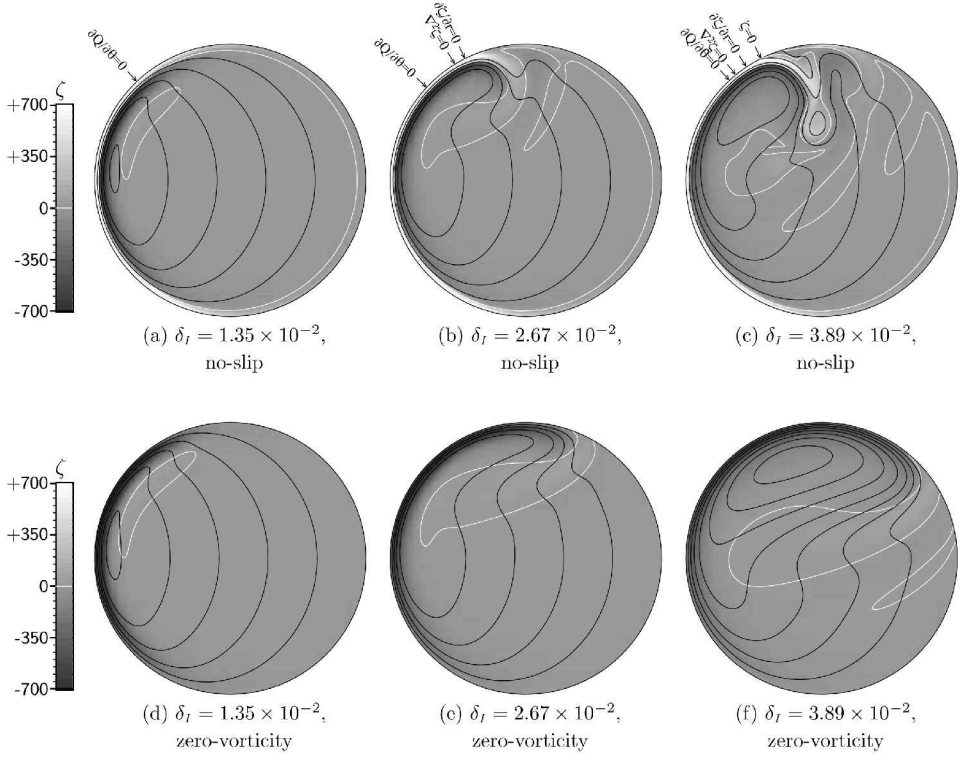

Figure 1. Flow under no-slip (top) and zero-vorticity (bottom) boundary conditions for various δ_I, with $\delta_S = 1.43 \times 10^{-2}$ and $\delta_M = 1.09 \times 10^{-2}$. The contour interval in ψ is $2.5 \times 10^{-3}\delta_S^{-1} = 0.175$. North is at the top, and the circulations are clockwise. Except for (c), all flows are steady. The grey shading indicates relative vorticity (paler corresponds to more cyclonic); the white contour separates cyclonic and anticyclonic regions. The labels indicate the westernmost points where $\partial Q/\partial\theta$, $\nabla^2\zeta$, $\partial\zeta/\partial r$ and ζ change sign as a function of azimuth near the boundary.

When $\delta_I \gg (\delta_M, \delta_S)$ the WBC is significantly altered by inertia. In the inflow region in the southwest an inertial boundary layer forms, with length scale δ_I and velocity and vorticity of $O(\delta_I^{-1})$ and $O(\delta_I^{-2})$, respectively (assuming there is no "inertial runaway" so the interior transport remains that predicted by the Sverdrup balance). When $\delta_M \neq 0$ there is also a thin sublayer (of thickness $(\delta_M^3/\delta_I)^{1/2}$) in which the tangential velocity is matched to the boundary condition (2.8) or (2.9) via a balance between lateral viscosity and advection. Under no-slip conditions this sublayer is cyclonic, with vorticity of $O(\delta_I^{-1/2}\delta_M^{-3/2})$.

Figure 1 shows how the streamline and vorticity structures evolve as the flow becomes more inertial under no-slip and zero-vorticity boundary conditions, with $\delta_S = 1.43 \times 10^{-2}$ and $\delta_M = 1.09 \times 10^{-2}$. Under these conditions the WBC has a mixed character intermediate between a Munk and Stommel layer in the linear limit, but with an oscillatory velocity profile. When $\delta_I = 0$ the circulation has a north-south symmetry (see the

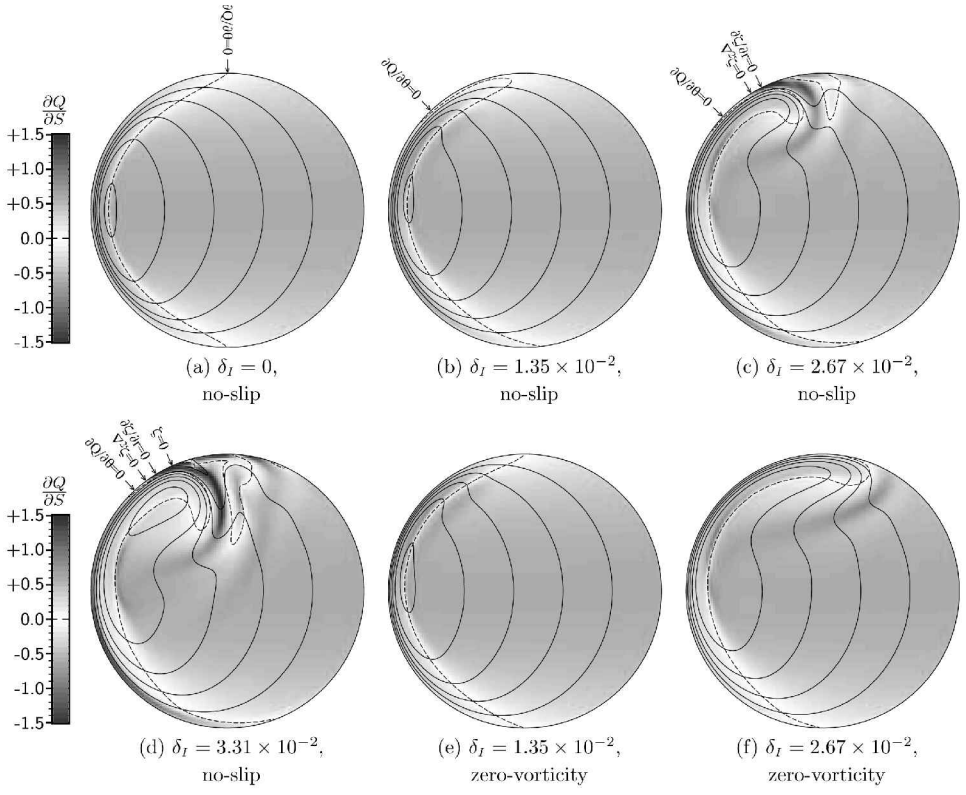

Figure 2. Loss and recovery of Q under no-slip (a–d) and zero-vorticity (e, f) boundary conditions and various δ_I, with $\delta_S = 1.43 \times 10^{-2}$ and $\delta_M = 1.09 \times 10^{-2}$. The contour interval in ψ is $2.5 \times 10^{-3}\delta_S^{-1} = 0.175$. North is at the top, and the circulations are clockwise and steady. The grey shading indicates the magnitude of $\partial Q/\partial S$; the dashed contour separates regions of positive and negative $\partial Q/\partial S$. The relative vorticity in (b, c, e, f) is shown in Figure 1 (a, b, d, e), respectively. The labels indicate the westernmost points where $\partial Q/\partial\theta$, $\nabla^2\zeta$, $\partial\zeta/\partial r$ and ζ change sign as a function of azimuth near the boundary.

streamlines in Fig. 2 (a)). When $\delta_I = 1.35 \times 10^{-2}$ (Figure 1 (a, d)) there is a slight northward intensification of the WBC. Under these weakly nonlinear conditions no-slip flows are virtually identical to those with a zero-vorticity boundary condition, the only noticeable difference being the cyclonic region of slower flow near the western boundary under no-slip conditions, which leads to a slight reduction in the overall transport. Streamlines leave the WBC across a broad range of latitudes in both cases. At larger δ_I the WBC outflow is quite different in the two models. With no-slip the WBC outflow veers sharply away from the coast as a concentrated jet. Initially this separation takes place without the formation of a stagnation point at the coast (Fig. 1 (b)), but at larger δ_I a stagnation point appears at the boundary north of the jet; when the forcing is sufficiently

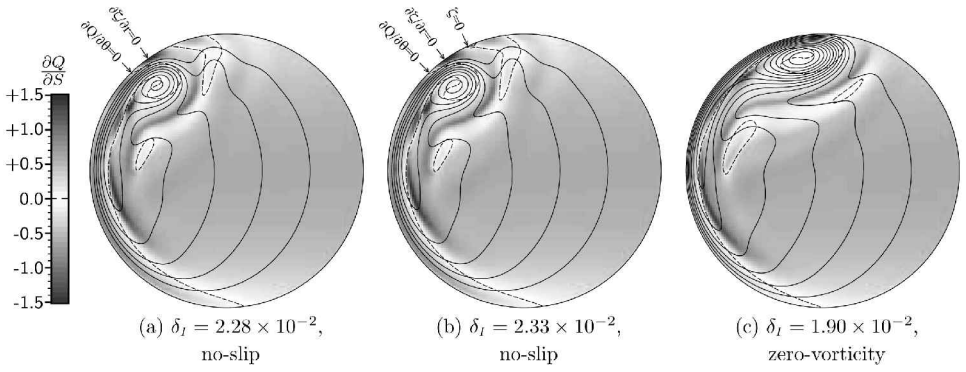

Figure 3. Loss and recovery of Q under no-slip (a, b) and zero-vorticity (c) boundary conditions and various δ_I, with $\delta_S = 0$ and $\delta_M = 2.00 \times 10^{-2}$. As for Figure 2 except the point where $\nabla^2\zeta = 0$ is not marked as it almost coincides with $\partial Q/\partial\theta = 0$.

strong the jet becomes unstable and sheds cyclonic eddies as in Figure 1 (c). Under zero-vorticity conditions the WBC separation occurs much later, and the outflow enters the interior as a relatively broad stream rather than a jet. Separation occurs further downstream as δ_I increases, in contrast to the no-slip case in which the separation point is almost independent of δ_I. The no-slip results are essentially the same as those found by Griffiths and Kiss (1999) in the sliced cylinder laboratory model. The sensitivity to boundary conditions is analogous to that observed by Blandford (1971) in a rectangular basin with nonuniform anticyclonic wind forcing and similar values of δ_S, δ_M and δ_I; in our case the contrasting separation behavior is shown in a "purer" form, since the confounding factors of basin corners and nonuniform forcing are absent.

Two different criteria can be used to characterize the onset of separation under no-slip boundary conditions (Becker and Page, 1990): [1] a change in sign of ζ at the boundary (this is the conventional criterion, indicating a stagnation point at the boundary and a region of reversed flow along the boundary), or [2] a change in sign of $\partial\zeta/\partial r$ at the boundary (indicating that the boundary vorticity extends into the interior). [2] is the weaker criterion, as it occurs at lower δ_I than that required to produce reversed flow (Griffiths and Kiss, 1999; Kiss, 2000). When both criteria are satisfied, the point at the boundary where $\partial\zeta/\partial r = 0$ is always upstream of the point where $\zeta = 0$. Points where ζ and $\partial\zeta/\partial r$ change sign at the boundary are marked in Figures 1–3 and 5–7 for no-slip flow. The flow in Figure 1 (a) does not satisfy either criterion; Figure 1 (b) shows separation by criterion [2] but not [1] (separation without a stagnation point), and Figure 1 (c) shows separation by both criteria. Under zero-vorticity boundary conditions criterion [2] is satisfied where the interior $\zeta = 0$ contour meets the boundary. However since this indicates a region of *zero* vorticity extending into the interior, it is dynamically different from the no-slip case in which the wall vorticity is strongly cyclonic.

b. Potential vorticity dynamics

In order to better understand the sensitivity to boundary conditions we will begin with a more detailed look at the separation process under zero-vorticity and no-slip conditions. The no-slip boundary condition demands a strongly cyclonic region against the lateral boundary, across which the anticyclonic azimuthal velocity is brought to rest,[4] thus the primarily anticyclonic WBC has a thin cyclonic sublayer next to the boundary. In contrast, with the zero-vorticity or free-slip condition the entire WBC is anticyclonic. We shall see that the alteration of the potential vorticity structure by the cyclonic region plays a key role in the separation process under the no-slip condition.

When $\delta_I = 0$ the potential vorticity Q has a simple linear dependence on y, and the point of maximum Q is located at the northernmost point of the boundary. Anticyclonic wind forcing reduces the Q of fluid columns as they drift southward in the Sverdrup interior. This Q is recovered via lateral and bottom friction in the WBC, allowing fluid columns to migrate northward to close the circulation. As δ_I increases, Q becomes increasingly modified by the relative vorticity of the flow. Since strong vorticity is confined to the WBC and the associated jet and recirculation, the Q modification takes place in these regions and the nearly irrotational Sverdrup interior is left essentially unaltered. Consequently, streamlines cannot leave the strongly vortical WBC region until their Q matches the *planetary* vorticity in the interior.

The locations where Q loss and recovery occur can be determined from plots of $\partial Q/\partial S$, the change in Q per unit arc length S along a streamline, which is equivalent to the gradient of Q in the direction of the velocity $\mathbf{u} = \hat{\mathbf{k}} \times \nabla\psi$:

$$\begin{aligned} \frac{\partial Q}{\partial S} &= \left(\frac{\mathbf{u}}{v}\right) \cdot \nabla Q \\ &= \frac{1}{v} J(\psi, Q) \\ &= \frac{1}{v} (W - \delta_S \zeta + \delta_M^3 \nabla^2 \zeta), \end{aligned} \tag{3.1}$$

where $v = |\mathbf{u}| = |\nabla\psi|$ is the flow speed and the third line follows from equation (2.5) in the steady state. The line integral of $\partial Q/\partial S$ around a closed streamline is zero, so all streamlines which pass through a region of nonzero $\partial Q/\partial S$ must also pass through a region where $\partial Q/\partial S$ has the opposite sign such that the line integrals through these regions cancel out. This integral property makes $\partial Q/\partial S$ a more useful diagnostic than $J(\psi, Q)$, the rate of change of Q per unit time for a fluid particle in a steady flow. Plots of $\partial Q/\partial S$ under various conditions are shown in Figure 2; the regions of Q loss and recovery are separated by the dashed contour $\partial Q/\partial S = 0$. In Figures 1 and 2 the azimuthal Q maximum near the

4. Green's theorem implies that the integrated vorticity is zero under no-slip conditions, so a strongly cyclonic region is required in order to cancel the anticyclonic vorticity in most of the basin.

boundary under no-slip conditions is also indicated[5]; under zero-vorticity conditions the Q maximum is always at the northernmost point.

When $\delta_I = 0$ the contour $\partial Q/\partial S = 0$ meets the boundary at the northernmost and southernmost points (see the dashed line in Figure 2 (a)) and Q recovery takes place relatively uniformly across the width of the WBC. At nonzero δ_I the recovery of Q is different in the cyclonic and anticyclonic regions of the WBC. The potential vorticity due to the relative vorticity in the WBC is of the same order as that due to the planetary vorticity when $\delta_I \sim \delta_M$ in the Munk limit $\delta_M \gg \delta_S$, or when $\delta_I \sim \delta_S$ or $\delta_I \sim \delta_S^{1/4}\delta_M^{3/4}$ in the anticyclonic or cyclonic regions in the Stommel limit $\delta_M \ll \delta_S$, or when $\delta_I \sim \delta_M$ in the frictional sublayer of an inertial boundary current; thus significant distortion to the Q contours can occur even for $\delta_I \ll 1$. In the outer WBC, Q is reduced by the anticyclonic relative vorticity (so Q contours are "dragged" northward), allowing fluid columns to delay their Q recovery while still moving northwards. That is, northward flow into increasingly negative ζ allows the advection term to compensate the β term in the local vorticity balance in the outer WBC inflow (as in an inertial boundary layer), reducing the imbalance of wind forcing and lateral and bottom friction, and therefore reducing $\partial Q/\partial S$ (see Eq. (3.1)). It can be seen in Figure 2 that strong Q recovery is delayed until the downstream part of the WBC, where ζ becomes less anticyclonic in the downstream direction and the advection and β terms therefore have the same sign. Thus, fluid columns in the anticyclonic region reach the northern end of the WBC with anomalously low Q relative to the interior; this effect, coupled with downstream advection of the vorticity structure, results in the eastward bulge in the $\partial Q/\partial S = 0$ contour in Figure 2 (f). At large δ_I this mismatch becomes so large that fluid columns must move *southward* around the eastern flank of a recirculation in order to find a latitude at which the planetary vorticity is sufficiently small for the flow to exit the WBC (see Fig. 1 (f)). Under zero-vorticity boundary conditions these considerations apply to the full width of the WBC, leading to the flow evolution illustrated in Figure 1 (d–f). This "crisis" of insufficient Q recovery and its role in driving the recirculation has been discussed by Cessi *et al.* (1987), Ierley and Young (1988) and Cessi (1990).

Under the no-slip condition fluid columns in the cyclonic region against the boundary face the opposite problem in terms of Q recovery at nonzero δ_I. In this region Q is increased (Q contours are deflected southward), and fluid columns in the WBC inflow must recover their potential vorticity sooner than in the linear case if they are to remain close to the boundary (i.e. the β and advection terms in the vorticity equation have the same sign, demanding a larger imbalance of wind forcing and lateral and bottom friction). This contrast between early and late Q recovery in the cyclonic and anticyclonic regions gives rise to the two-layered $\partial Q/\partial S$ structure in the inflow regions in Figure 2 (b–d) (particularly

5. The azimuthal Q maximum depends strongly on r near the boundary; the label corresponds to the Q maximum one grid point from the boundary (as in Figure 4) and gives a fair indication of where Q begins to decrease downstream in the cyclonic region. The location where $\nabla^2\zeta = 0$ is also determined at this radius.

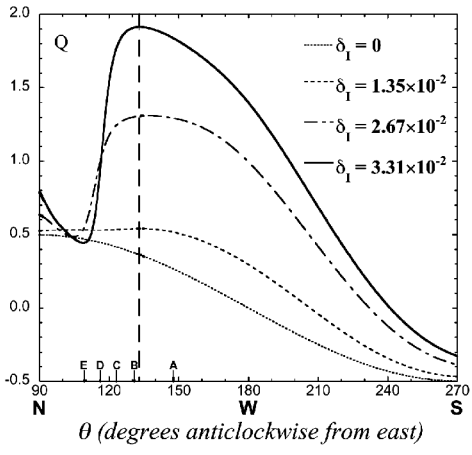

(a) Potential vorticity Q

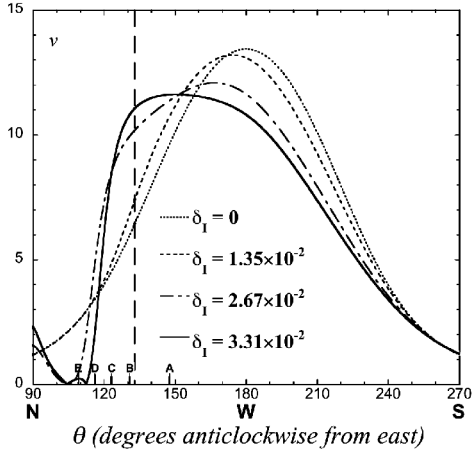

(b) Flow speed $v \equiv |\mathbf{u}|$

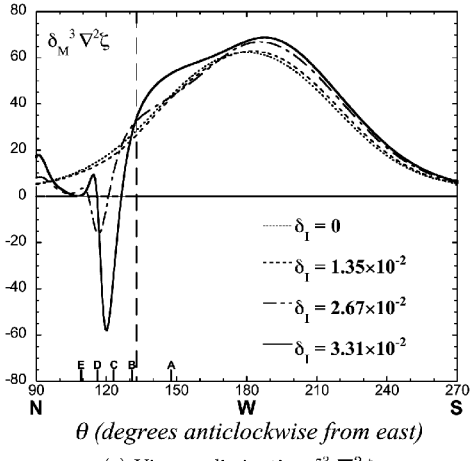

(c) Viscous dissipation $\delta_M^3 \nabla^2\zeta$

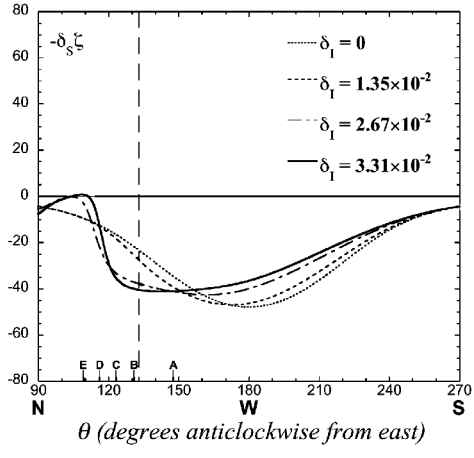

(d) Bottom friction $-\delta_S\zeta$

Figure 4. Azimuthal profiles at $r = 0.497$ (one grid cell from the boundary) in the WBC under no-slip boundary conditions with $\delta_S = 1.43 \times 10^{-2}$, $\delta_M = 1.09 \times 10^{-2}$, and various δ_I corresponding to some of the flows shown in Figures 1–7. The dashed vertical lines indicate the onset of Q reduction for $\delta_I = 3.31 \times 10^{-2}$. Radial profiles with $\delta_I = 3.31 \times 10^{-2}$ are shown in Figure 5 at the positions marked A–E.

at large δ_I), compared to the linear case in Figure 2 (a) and the flows with a zero-vorticity boundary condition in Figure 2 (e, f).

Figure 4 (a) shows azimuthal profiles of Q one grid cell from the boundary for various values of δ_I; these curves have slopes of approximately $-0.5\partial Q/\partial S$ in regions where the flow is very nearly azimuthal ($\partial Q/\partial S$ will however be disproportionately sensitive to the radial velocity since Q depends strongly on r). It is evident that under weakly nonlinear

conditions ($\delta_I = 1.35 \times 10^{-2}$ in our case) the cyclonic boundary vorticity is sufficient to shift the Q maximum westward,[6] so that the $\partial Q/\partial S = 0$ contour loops back around the anticyclonic part of the WBC outflow (see Fig. 2 (b)), in contrast to the corresponding flow with a zero-vorticity boundary condition (see Fig. 2 (e)). This indicates that the fluid in the cyclonic layer has recovered more Q than it requires to rejoin the interior, so the WBC outflow beyond this point must take place in a way that allows this excess to be dissipated.

Under more inertial conditions (Fig. 2 (c, d)) it is clear from Figure 4 (a) that the Q maximum in the cyclonic sublayer far exceeds that in the interior and very strong potential vorticity dissipation is needed (note that there is nowhere in the interior where the planetary vorticity shown by the $\delta_I = 0$ curve matches the large boundary value of Q, in contrast to the anticyclonic outer WBC in which insufficient Q recovery can be compensated by a southward extension of the WBC to find a latitude of matching planetary vorticity). With larger δ_I the cyclonic vorticity maximum is advected farther north (see Fig. 4 (d)), and Q loss occurs very abruptly in a small region near $\theta = 120°$ (Fig. 4 (a)). There is strong deceleration in this region, and strongly negative viscous dissipation (Fig. 4 (b, c)). It will be shown in the following section that the vorticity structure required for this strong Q dissipation leads to separation of the cyclonic region, which in turn guides the whole WBC away from the coast. This offshore flow advects the boundary vorticity into the interior to form a jet.

The features of the WBC vorticity structure which lead to separation are not sensitive to the value of δ_S, since a cyclonic sublayer will always be present when $\delta_M \neq 0$ and the no-slip condition is chosen. This point is illustrated in Figure 3, which shows the structure of $\partial Q/\partial S$ for flows with $\delta_S = 0$ (i.e. no bottom friction). Note that the cyclonic and anticyclonic regions have a similar width and therefore a similar vorticity magnitude in these nonlinear Munk boundary layers, in contrast to a Stommel boundary current in which the cyclonic vorticity is much stronger. This effect and the smaller value of δ_I lead to a less conspicuous two-layer structure for $\partial Q/\partial S$ under no-slip conditions than in Figure 2 (c, d).

c. Dissipation of the potential vorticity excess

Having established that fluid columns in the cyclonic sublayer of an inertial-viscous WBC acquire more potential vorticity than is needed to re-enter the interior, we will now look at the changes to the flow structure which allow this excess potential vorticity to be dissipated. We will focus on the region upstream of any separation by criterion [1], where the flow along the boundary is northward and the no-slip condition implies $\zeta > 0$ at the boundary.

Figure 4 (b–d) shows azimuthal profiles, one grid cell from the boundary, of the dominant terms on the right-hand side of equation (3.1) in the cyclonic sublayer. Radial profiles in the WBC outflow at the azimuthal positions marked A–E are shown in Figure 5

6. The actual shift depends on the variation of ζ with azimuth, but we expect it to be significant when $\delta_I \sim \delta_M$ (in the Munk limit or the viscous sublayer of an inertial WBC), or when $\delta_I \sim \delta_S^{1/4}\delta_M^{3/4}$ (in the Stommel limit).

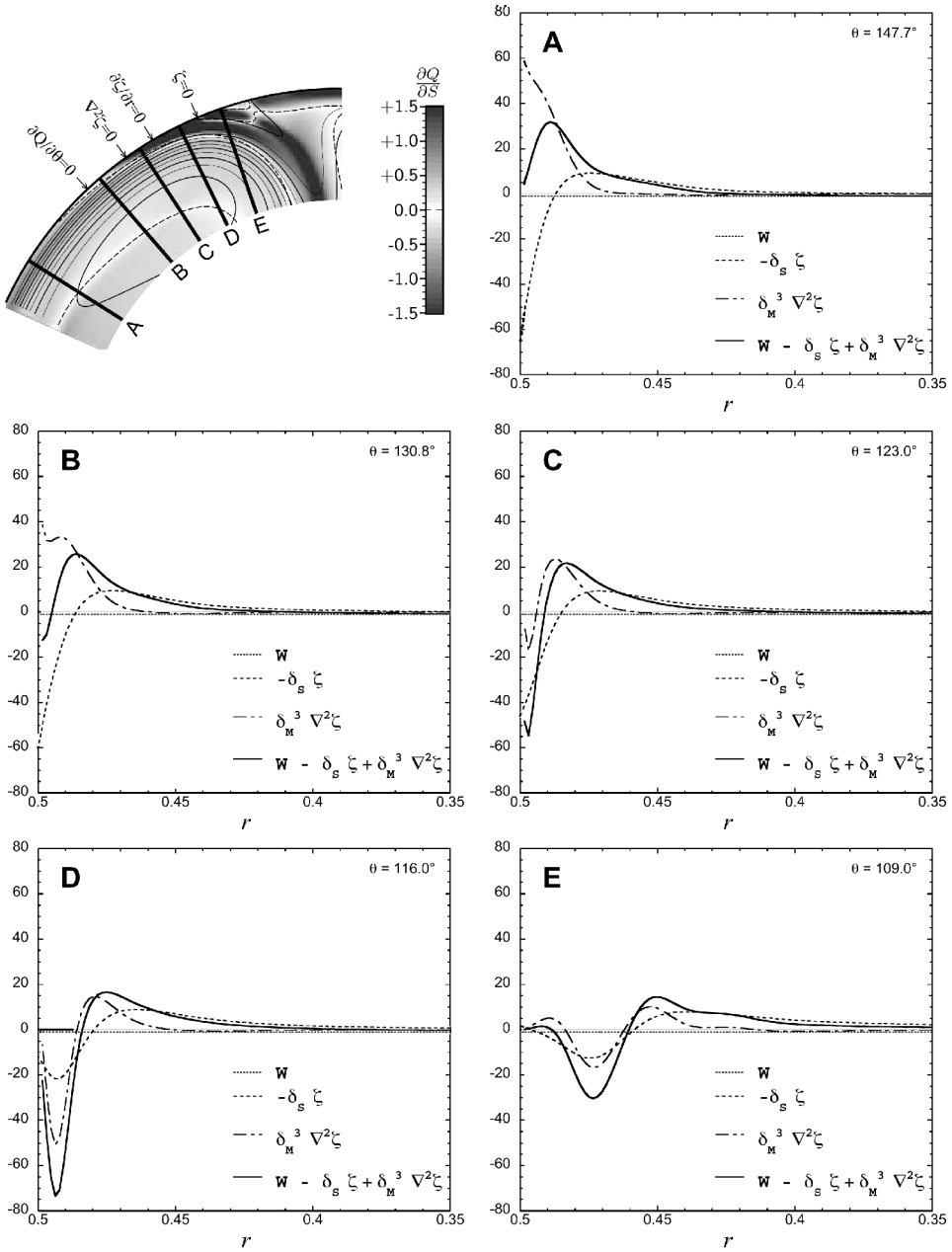

39

Figure 5. Radial profiles of terms in equation (3.1) (not divided by the flow speed) under no-slip boundary conditions, with $\delta_S = 1.43 \times 10^{-2}$, $\delta_M = 1.09 \times 10^{-2}$, and $\delta_I = 3.31 \times 10^{-2}$. The r axes are reversed so the boundary is at the left in the profiles. A key to the location and width of the profiles is shown at top left (with a ψ contour interval of $1.25 \times 10^{-3}\delta_S^{-1} = 8.74 \times 10^{-2}$ but otherwise as in Figure 2). This calculation used 320 radial grid points (twice the usual resolution) to obtain smooth profiles, but the flow is essentially identical to that obtained with 160 grid points (see Figure 2 (d); note the different contour interval).

for $\delta_I = 3.31 \times 10^{-2}$. In the boundary layer we have $\nabla^2\zeta \approx \partial^2\zeta/\partial r^2$, so changes to the radial vorticity profile (shown by $-\delta_S\zeta$ in Figure 5) can be related directly to changes in the viscous term.

i. The onset of Q reduction: $\nabla^2\zeta$ decreases. In the inflow region of the sublayer ζ and $\nabla^2\zeta$ are positive whilst W is negative (and negligible in comparison), and $W - \delta_S\zeta + \delta_M^3\nabla^2\zeta > 0$, so $\partial Q/\partial S > 0$ from equation (3.1) (see profile A in Figure 5). It is evident from equation (3.1) that reduction of Q requires $W - \delta_S\zeta + \delta_M^3\nabla^2\zeta < 0$, but at first glance it is difficult to say *a priori* whether this will take place by $\delta_M^3\nabla^2\zeta$ becoming less positive, or $-\delta_S\zeta$ becoming more negative. Using equation (3.1), the definition of Q and the spatial uniformity of W we find that the downstream variation of $\partial Q/\partial S$ is given by

$$\frac{\partial^2 Q}{\partial S^2} = \frac{1}{v}\left[\frac{\delta_S}{\delta_I^2}\frac{\partial y}{\partial S} - \left(\frac{\delta_S}{\delta_I^2} + \frac{\partial v}{\partial S}\right)\frac{\partial Q}{\partial S} + \delta_M^3\frac{\partial \nabla^2\zeta}{\partial S}\right]. \tag{3.2}$$

In the northward-flowing cyclonic sublayer we have $\partial y/\partial S > 0$. The second term vanishes where $\partial Q/\partial S$ changes sign, so we must have $\delta_M^3(\partial\nabla^2\zeta/\partial S) < -(\delta_S/\delta_I^2)(\partial y/\partial S) \leq 0$ in order to obtain $\partial^2 Q/\partial S^2 < 0$ at this point, i.e. $\nabla^2\zeta$ must decrease downstream across the $\partial Q/\partial S = 0$ contour (at a finite rate if $\delta_S \neq 0$) in order to obtain $W - \delta_S\zeta + \delta_M^3\nabla^2\zeta < 0$ in the sublayer outflow. Physically, this is because $\partial Q/\partial S = \delta_I^2(\partial\zeta/\partial S) + (\partial y/\partial S)$, so in the region where Q decreases downstream despite northward flow we have $\delta_I^2(\partial\zeta/\partial S) < -(\partial y/\partial S) < 0$, i.e. ζ decreases downstream at a finite rate, so the bottom friction $-\delta_S\zeta$ becomes *less* negative downstream across the contour $\partial Q/\partial S = 0$. These changes to these terms are evident in Figure 4 (c, d).

When fluid columns first pass into the Q dissipation region, $\partial Q/\partial S$ becomes negative via a subtle change to the radial profile of the vorticity which reduces $\delta_M^3\nabla^2\zeta$ below $\delta_S\zeta - W$ but does not change its sign (see profile B in Fig. 5). At small δ_I this low rate of Q loss is sufficient to adjust the potential vorticity of fluid columns to a value which allows them to re-enter the interior and no more drastic alterations are needed, so the outflow retains the same qualitative structure as in the linear case (see Fig. 2 (b) and the corresponding profiles with $\delta_I = 1.35 \times 10^{-2}$ in Fig. 4).

At larger δ_I the Q surplus is larger and $\partial Q/\partial S$ must become more negative in the sublayer outflow. From equations (3.1) and (3.2) it is evident that when $\partial Q/\partial S < 0$ a further decrease in $\partial Q/\partial S$ downstream can be obtained via a progressive decrease in either $\nabla^2\zeta$ or the flow speed v. However on a streamline $\psi = \psi_c$ a small distance l from the no-slip boundary we have $v \approx 2|\psi_c|/l$ (assuming a near-linear cross-stream velocity profile), so under the boundary-layer approximation $|\zeta| \approx v/l \approx v^2/|2\psi_c|$. Therefore v cannot vary along a streamline independently of ζ and Q (compare Figures 4 (a), (b) and (d)). On the other hand, since $\nabla^2\zeta \approx \partial^2\zeta/\partial r^2$, relatively subtle changes to the radial vorticity profile allow the lateral viscosity to fall rapidly downstream even when Q is large. Thus a further decrease in $\partial Q/\partial S$ downstream initially takes place primarily via a rapid reduction in $\nabla^2\zeta$; as Q becomes smaller downstream so does v and this reduces $\partial Q/\partial S$

further. Rapid deceleration therefore occurs downstream of an abrupt fall in $\nabla^2\zeta$; this characteristic feature can be seen in Figure 4 (b, c): $\nabla^2\zeta$ falls rapidly to a minimum (eg. at $\theta \approx 120°$ for $\delta_I = 3.31 \times 10^{-2}$) where the relatively swift flow experiences its strongest deceleration.

ii. Strong Q reduction: $\nabla^2\zeta < 0$. It can be seen in Figures 4 and 5 that $\nabla^2\zeta$ drops below zero in the Q dissipation region under strongly inertial conditions; the point where $\nabla^2\zeta = 0$ is also indicated in Figures 1 and 2.

The origin of this feature is obvious in the Munk limit $\delta_S \ll \delta_M$, since $\partial Q/\partial S < 0$ is equivalent to $\delta_M^3\nabla^2\zeta < 0$ apart from the negligible effect of wind forcing (see equation (3.1)). Thus $\nabla^2\zeta$ vanishes at almost the same point as $\partial Q/\partial S$ in Figure 3 and it is therefore not marked.

When bottom friction also contributes to Q dissipation $\nabla^2\zeta$ need not become negative as soon as $\partial Q/\partial S < 0$, and may not change sign at all. Note however that since the Q excess grows as $\delta_I^2\zeta$, the bottom friction $-\delta_S\zeta$ becomes an increasingly inadequate mechanism for Q dissipation as δ_I increases (see Fig. 4 (a, d)). Lateral viscosity must therefore assume an increasingly important role in Q dissipation, eventually requiring $\nabla^2\zeta < 0$. Although the exact conditions under which this occurs are difficult to determine, the following simple argument suggests an upper bound for δ_I (dependent on δ_M and δ_S) beyond which $\nabla^2\zeta$ cannot remain positive throughout the WBC outflow. Neglecting the relatively unimportant role of the β effect, the dissipation of a sublayer vorticity excess $\Delta Q = \delta_I^2\zeta$ purely by bottom friction on a streamline $\psi = \psi_c$ is governed by the equation $\partial\zeta/\partial S = -\delta_S\zeta/\delta_I^2 v \approx -(\delta_S/\delta_I^2\sqrt{2|\psi_c|})\zeta^{1/2}$ near the no-slip boundary, since $v \approx \sqrt{2|\psi_c|\zeta}$. This yields the quadratically decaying solution

$$\zeta(S) = \begin{cases} \dfrac{\delta_S^2}{8\delta_I^4|\psi_c|}(S_0 - S)^2 & \text{if } S \le S_0 \\ 0 & \text{if } S > S_0 \end{cases}. \tag{3.3}$$

Thus deceleration allows bottom friction to extinguish the relative vorticity in a finite distance given by the constant of integration S_0. At $S = 0$ we can rearrange (3.3) to obtain $S_0 = \delta_I^2\sqrt{8|\psi_c|\zeta(0)}/\delta_S \approx 2\delta_I^2 v(0)/\delta_S$. If we define $S = 0$ to be the location of the vorticity maximum on $\psi = \psi_c$, the flow speed $v(0)$ at this point will be that given in Section 3a on streamlines in the outer part of the cyclonic sublayer: $v(0) = O(\delta_S^{-1})$ in the Stommel limit, $v(0) = O(\delta_M^{-1})$ in the Munk limit, and $v(0) = O(\delta_I^{-1})$ in an inertial WBC. In all three cases it is clear that when $\delta_I \gg (\delta_S, \delta_M)$ we require $S_0 \gg 1$ and there is not enough room in the basin for ΔQ to be dissipated entirely by bottom friction. If $\delta_M^3\nabla^2\zeta > 0$ dissipation of this additional Q input requires a distance in excess of S_0.

iii. Very strong Q reduction: $\nabla^2\zeta \ll 0$ *leads to separation.* It is possible to have $\nabla^2\zeta < 0$ while retaining the radial vorticity maximum at the boundary (see profile C in Fig. 5), but very strong dissipation of Q demands $\nabla^2\zeta \ll 0$, which tends to result in a vorticity profile

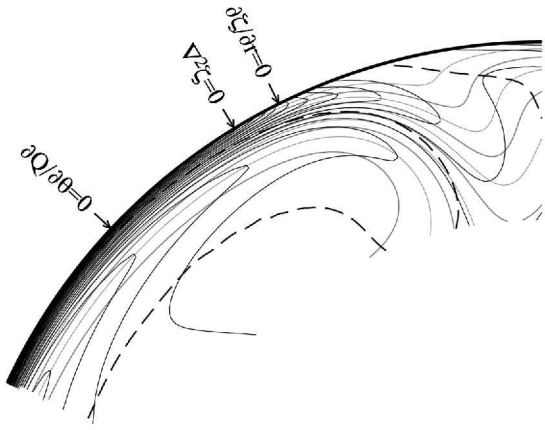

Figure 6. Separation due to steering by the potential vorticity structure, for no-slip flow with $\delta_S = 1.43 \times 10^{-2}$, $\delta_M = 1.09 \times 10^{-2}$, and $\delta_I = 2.67 \times 10^{-2}$ (as in Figure 1 (b) and Figure 2 (c)). Contours of Q (black, CI = 0.1) and $|\psi|^{1/2}$ (grey, CI = 2.185×10^{-2}) are shown, and the dashed curve is the contour $\partial Q/\partial S = 0$. Separation occurs without a stagnation point in this case. Contours of $|\psi|^{1/2}$ are plotted in order to show the streamlines in the nearly stagnant region at the boundary downstream of the separation.

with a maximum away from the boundary (profile D). The reason for this can be seen by applying Gauss' theorem to a box of negligible azimuthal extent $\Delta\theta$ with radial boundaries at the wall and somewhere in the cyclonic sublayer. This yields

$$\frac{1}{r|_{wall}}\Delta\theta\int\int \nabla^2\zeta dA \simeq \frac{\partial\zeta}{\partial r}\Big|_{wall} - \frac{\partial\zeta}{\partial \mathrm{r}}\Big|_{sublayer}, \tag{3.4}$$

since the azimuthal fluxes will cancel if the box is sufficiently small in the azimuthal direction relative to the azimuthal length scale of the flow. Upstream of the region where $\partial Q/\partial S < 0$ we have $\partial\zeta/\partial r|_{wall} > \partial\zeta/\partial r|_{sublayer} > 0$, so $\int\int \nabla^2\zeta dA > 0$. Initially $\int\int \nabla^2\zeta dA$ becomes negative by a reduction of $\partial\zeta/\partial r|_{wall}$, so $\partial\zeta/\partial r|_{sublayer} > \partial\zeta/\partial r|_{wall} > 0$. However to obtain $\int\int \nabla^2\zeta dA \ll 0$ the wall vorticity gradient must drop even further (because $\partial\zeta/\partial r|_{sublayer}$ is also becoming smaller as ζ is reduced), and we ultimately require $\partial\zeta/\partial r|_{wall} < 0$. This implies a vorticity profile in which the ζ maximum has separated from the boundary, as seen in profile D in Figure 5 and in Figure 1 (b, c) past the point marked $\partial\zeta/\partial r = 0$.

The change in sign of $\partial\zeta/\partial r$ at the boundary is flow separation by criterion [2]. Since $\partial Q/\partial r \approx \delta_I^2\partial\zeta/\partial r$ in the WBC outflow, separation of the vorticity maximum implies that the region of large Q also bulges out from the boundary. By definition, streamlines in the region where $\partial Q/\partial S < 0$ must cross potential vorticity contours in the direction of decreasing Q; as a result, the streamlines on the seaward side of the bulge are guided away from the boundary, as shown in Figure 6. The anticyclonic outer part of the WBC is also

deflected offshore as a result. When the resulting offshore flow is sufficiently inertial it advects the layers of positive and negative ζ into the interior to form a jet (see Fig. 1 (b, c)). In contrast the fluid very close to the sidewall ends up on the shoreward side of the bulge in the Q contours past the point where $\partial\zeta/\partial r = 0$. This fluid does not separate (at least at first) but creeps northward near the boundary in the nearly stagnant region north of the separated jet (by continuity the offshore flow of the bulk of the WBC is associated with widening of streamtubes, and therefore deceleration, near the boundary). Very little fluid takes this second route under the conditions shown (see Fig. 1 (b)), so contours of $|\psi|^{1/2}$ were plotted in Figure 6 in order to show the streamlines. At larger δ_I the vorticity drops below zero at some point in this nearly stagnant region, giving separation by criterion [1]. This appears to be a finite-amplitude effect which is not fundamental to the WBC separation process; indeed Griffiths and Kiss (1999) observed an extensive regime in which the WBC separated by criterion [2] but not [1].

d. Pressure gradient

In the steady state the component of the momentum equation (2.1) in the direction of flow can be written

$$-\frac{\partial p}{\partial S} + \tau_{\|} = \delta_I^2 \nu \frac{\partial v}{\partial S} + \delta_S \nu - \delta_M^3 \mathcal{V}_{\|}, \tag{3.5}$$

where $\nu = |\mathbf{u}|$ as before, $\tau_{\|} = \mathbf{u} \cdot \tau/\nu$, $\mathcal{V}_{\|} = (\mathbf{u} \cdot \nabla^2\mathbf{u})/\nu$ and S is the arc length along a streamline in the direction of flow. $\partial p/\partial S$ is a residual ageostrophic pressure gradient because the gradient of the dominant geostrophic component is identically zero in the streamwise direction.

In the formulation used here, the flow pattern is determined entirely by the vorticity equation (2.5), and therefore depends only on $W = \hat{\mathbf{k}} \cdot \nabla \times \tau$. The flow will not be altered if we add an irrotational field (i.e. $\nabla\phi$, for any scalar field ϕ) to τ (since $\nabla \times \nabla\phi = 0$), and the additional forcing must therefore be balanced by a change in ∇p in the momentum equation (2.1) since the other terms do not change. Thus only $\nabla p - \tau$, not ∇p itself, can be determined uniquely from a solution to the vorticity equation (2.5). However the flow obtained with a wind stress τ is identical to that obtained with $\tau' = \tau - \tau(x_0, y_0)$, since the constant field $\tau(x_0, y_0)$ is irrotational. For this flow we have $\nabla p - \tau = \nabla p' - \tau' = \nabla p'$ at the point (x_0, y_0). Thus at any given point $\nabla p - \tau$ plays the role of a pressure gradient in an equivalent flow; we can use this argument to justify referring loosely to $\nabla p - \tau$ as a "pressure gradient." In the frequently-used configuration of a purely zonal wind stress and a meridional western boundary these subtleties can be ignored, since $\tau_{\|} = 0$ close to the wall.

Figure 7 shows the streamwise component of the "pressure gradient" force $-\nabla p + \tau$ calculated from (3.5) for the same flow as in Figure 6 (once again contours of $|\psi|^{1/2}$ are plotted). The "pressure gradient" force is "favorable" (i.e. acting in the direction of flow) in

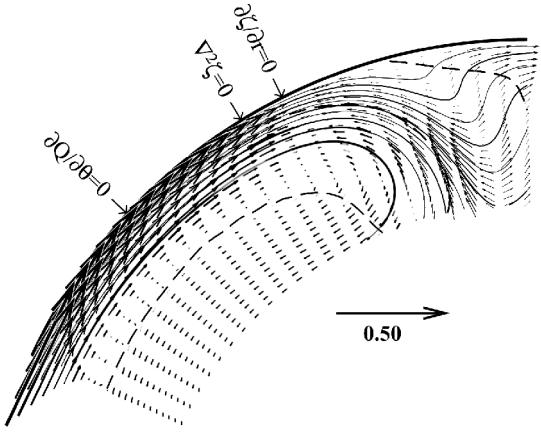

Figure 7. The streamwise component of $-\nabla p + \tau$, for no-slip flow with $\delta_S = 1.43 \times 10^{-2}$, $\delta_M = 1.09 \times 10^{-2}$, and $\delta_I = 2.67 \times 10^{-2}$ (as in Figures 1 (b), 2 (c) and 6). Vectors are shown for every second radial and every fourth azimuthal grid point. Streamlines (contours of $|\psi|^{1/2}$) are shown as in Figure 6, and the dashed curve is the contour $\partial Q/\partial S = 0$.

most of the WBC, but becomes "adverse" (opposing the flow) near the boundary where $\partial\zeta/\partial r$ is negative.

This connection between the radial vorticity gradient and the streamwise "pressure gradient" follows from the momentum balance at the no-slip boundary, where we have

$$-\left.\frac{\partial p}{\partial S}\right|_{wall} + \tau_{\|}|_{wall} = -\delta_M^3 \mathscr{V}_{\|}|_{wall}, \tag{3.6}$$

since the other terms in (3.5) vanish. Assuming clockwise azimuthal flow (so $\zeta|_{wall} = -\partial v/\partial r|_{wall}$), we have $-\mathscr{V}_{\|}|_{wall} = -\partial^2 v/\partial r^2|_{wall} - (1/r)\partial v/\partial r|_{wall} = \partial\zeta/\partial r|_{wall} + \zeta/r|_{wall}$ at a no-slip radial boundary. Under the boundary-layer approximation the first term is dominant and the momentum balance (3.6) along the wall is

$$-\left.\frac{\partial p}{\partial S}\right|_{wall} + \tau_{\|}|_{wall} = \delta_M^3 \left.\frac{\partial\zeta}{\partial r}\right|_{wall}. \tag{3.7}$$

Thus separation by criterion [2] will always be associated with an adverse "pressure gradient"; this result is also obtained for non-rotating fluids (see Tritton, 1988, section 12.2).

The adverse "pressure gradient" in the separation region is reminiscent of the situation in non-rotating flows at large Reynolds number (eg. Schlichting, 1968), in which viscous boundary layers separate due to deceleration by an adverse pressure gradient imposed by the inviscid flow outside the boundary layer. We can use the width and velocity of the WBC to obtain a Reynolds number $Re = \delta_I^2/\delta_M^3$, which is moderately large for the separated flows studied here (eg. $Re = 546$ and 840 in Figure 2 (c) and (d), respectively).

However it can be seen in Figure 7 that the "pressure gradients" originate within the WBC itself (where both the viscous and inertial terms are significant), rather than being constant across the boundary layer and determined by a balance with inertia alone outside the viscous layer. Thus in our case separation by criterion [2] cannot be understood by analogy with non-rotating flow as due to deceleration by an adverse "pressure gradient" imposed by an external inviscid flow. In fact deceleration begins well upstream of the adverse "pressure gradient" region, since $\partial\zeta/\partial S < 0$ implies $\partial v/\partial S < 0$ near the no-slip boundary. Thus deceleration begins slightly upstream of the point marked $\partial Q/\partial\theta = 0$ in Figure 7, where the "pressure gradient" is strongly favorable but not strong enough to balance the viscous drag in equation (3.5). We note however that the adverse "pressure gradient" arising in the separated viscous-inertial jet does appear to be imposed onto the nearly stagnant region to its north, and speculate that when this is sufficiently strong it may drive the reversed flow characteristic of separation by criterion [1].

4. Discussion and conclusions

The results and analysis of the previous section have shown how the vorticity dynamics of the cyclonic sublayer can dramatically alter the WBC outflow under the no-slip condition compared to the flow with a zero-vorticity boundary condition in which this sublayer is absent. With no-slip there is a "crisis" of excessive Q recovery in the sublayer which prevents the WBC from assuming the form taken under zero-vorticity boundary conditions, in which it continues along the boundary until the outer WBC has recovered sufficient Q. This explains why the outflow structure is so different, despite a similar potential vorticity deficit occurring in the anticyclonic part in both cases. When the boundary is straight or concave the cyclonic sublayer will be absent under a free-slip (i.e. zero-stress) boundary condition and the flow will closely resemble that found here with a zero-vorticity boundary condition.

With anticyclonic wind forcing the basic argument is

1. The cyclonic WBC sublayer occurring with no-slip conditions is a region of high potential vorticity Q.
2. The sublayer outflow must assume a configuration which allows this Q excess to be dissipated before fluid columns re-enter the interior.
3. Q dissipation must take place by the lateral viscous term $\delta_M^3\nabla^2\zeta$ becoming less positive (even in the presence of bottom friction).
4. Strongly inertial outflows have a very large Q excess, requiring $\delta_M^3\nabla^2\zeta \ll 0$.
5. $\delta_M^3\nabla^2\zeta \ll 0$ yields $\partial\zeta/\partial r < 0$, producing a Q structure which guides the sublayer offshore and implying an adverse "pressure gradient" in the sublayer.
6. The offshore flow in turn drives the outer anticyclonic WBC offshore, so vorticity of both signs is advected into the interior to form a jet.

This separation mechanism differs from that suggested previously (Holland and Lin, 1975) in that the potential vorticity "crisis" occurs in the sublayer due to an excessive recovery of Q, rather than in the outer boundary current due to insufficient Q recovery. With Laplacian lateral friction a change in sign of $\partial\zeta/\partial r$ at the boundary is fundamental to this WBC separation process, and a necessary precursor to separation with stagnation (a change in sign of ζ at the boundary). From this point of view the formation of a stagnation point is of little fundamental importance, as it is simply a finite-amplitude expression of the vorticity dynamics required for the vorticity maximum to leave the boundary. Thus criterion [2] ($\partial\zeta/\partial r = 0$) or $\partial Q/\partial r = 0$ can be better indicators of separation than a stagnation point at the boundary, because in a rotating flow they imply a Q structure which guides the sublayer offshore.

Note that the separation process described here requires only lateral viscosity, vorticity advection and an ambient potential vorticity gradient, so the arguments presented above apply equally well if $\delta_S = 0$ and/or $W = 0$. Analogous potential vorticity considerations also apply under cyclonic forcing ($W > 0$), causing separation of the WBC outflow in the southwest at large δ_I. The general mechanism does not depend on the particular formulation or boundary shape used here and is likely to be involved in the western boundary current separation observed in other barotropic models.

Excessive Q recovery in the viscous sublayer is expected to be a feature of most barotropic models under no-slip conditions when the flow is sufficiently inertial. This feature was noted by Cessi *et al.* (1990) in a barotropic regional model driven by prescribed inflow and outflow, and is also seen in the potential vorticity structure of flow in a similar model reported by Cessi (1991).

The manner in which the flow deals with this excess Q recovery depends on which potentially dissipative terms are present in the model. If lateral friction (of whatever form) assumes this role, we expect it to change sign near the outflow. A close association between separation and such a change in sign of the viscous term was noted by Moro (1988) in a two-gyre barotropic model in a rectangular domain with a no-slip boundary. In a two-gyre model there may also be some cancellation (by a viscous flux or eddy transport) of the opposite-signed vorticity excesses in the two western boundary current sublayers where they meet after separation.

In models which use Laplacian lateral friction we expect a change in sign of the friction term to be closely associated with a change in sign of the vorticity gradient normal to the boundary; this is evident in the results of Moro (1988) and Cessi (1991). The flow in both models closely resembles that described here, showing that this separation process can operate in a rectangular domain and is therefore not reliant on boundary curvature or its inclination to the planetary vorticity gradient. With Laplacian friction a change in sign of the vorticity gradient normal to the boundary will result in an adverse pressure gradient along the wall, and this can also be inferred from the results of Moro (1988) and Cessi (1991) (in both cases $\tau_{||} = 0$ at the western boundary). In this context it is important to distinguish between the pressure gradient (3.7) which actually occurs at the wall, and the

gradient imposed by the flow outside the WBC, described by Cessi (1991) and Pedlosky (1996, section 2.6). The latter can give a misleading indication of the pressure gradient along the wall near separation because flow structures such as recirculations, countercurrents and standing Rossby waves also impose strong pressure gradients along the wall (see Appendix).

We might expect this separation mechanism to be less applicable in a stratified flow due to the dependence of the potential vorticity on isopycnal separation. However a hint of further generality is given by the concordance of these results with those obtained by Haidvogel *et al.* (1992) using a stratified three-level eddy-resolving double-gyre model with biharmonic lateral friction. Haidvogel *et al.* (1992) observed a systematic retreat of the (time-mean) separation points from the zero wind curl line as the boundary condition changed from slip to no-slip, that is, as the sublayer became more strongly cyclonic (anticyclonic) in the subtropical (subpolar) gyre. This change was associated with the injection of negative (positive) potential vorticity by the biharmonic viscous stress at the wall close to the separation point in the subtropical (subpolar) gyre at the upper level under no-slip conditions. This is analogous to the region with $\nabla^2\zeta \ll 0$ in the model discussed here (and probably results from a similar need to compensate for excessive Q recovery in the sublayer), but the connection with separation is less clear due to the use of biharmonic friction. Haidvogel *et al.* (1992) also found that separation takes place in a region of adverse pressure gradient. It is possible that the separation process is not crucially dependent on the form of the lateral friction, because $\zeta \propto v^2$ on a streamline near the boundary under the no-slip condition, so strong Q dissipation involves rapid streamwise deceleration, implying streamtube widening and offshore flow.

It is possible that a similar process plays a role in WBC separation in the oceans, although the dynamics are likely to be much more complex due to the effects of topography and stratification. These give rise to additional terms in the potential vorticity balance which may modify the potential vorticity of the sublayer or reduce the extent to which strong negative lateral "viscous" (actually turbulent) diffusion is required. The separation process identified in the present paper hinges on the dynamics which operate in the thin cyclonic sublayer at the western boundary; it is therefore evident that this layer must be adequately resolved for an ocean model to correctly reproduce this behavior. Verron and Blayo (1996) have shown that the type and location of separation (in a three-layer two-gyre model) can depend strongly on the numerical implementation used for the no-slip condition when the resolution of the sublayer is poor (that is, when the vorticity excess and its dissipation are inaccurately calculated).

Although the analysis presented here explains many of the features observed in barotropic WBC separation, it does not provide a method for predicting the separation point *a priori*. It is likely that this will depend on the detailed vorticity balances in the outflow and will be difficult to predict unless there is a strong topographic or boundary feature (such as a cape) which favors separation at a particular location (eg. Dengg, 1993).

In an eddy-resolving model without such features the separation point is likely to be time-dependent (Haidvogel *et al.,* 1992).

Acknowledgments. Support for this work was provided by an Australian Research Council Postdoctoral Fellowship (F00104281). I thank the anonymous referees for comments which led to an improved manuscript.

APPENDIX

A reassessment of pressure gradients in the results of Cessi (1991)

Using an analysis based on integration of the boundary layer equations from the wall into the interior, Cessi (1991) derived an expression equating the longshore pressure gradient at the wall with the value of the streamfunction in the far field, and concluded that the WBC could separate before reaching the region of adverse pressure gradient (this formula was also obtained by Pedlosky, 1996, section 2.6). However this derivation assumes that the boundary layer vorticity equation is applicable everywhere between the boundary and the region where the streamfunction is Sverdrupian (or given by the outflow conditions as in Cessi, 1991). This is a reasonable approximation far from the separation region, but is not valid close to separation, where the flow contains structures such as recirculations, countercurrents and standing Rossby waves in the region between the wall boundary layer and the interior. These flow structures can significantly modify the pressure gradient impressed on the boundary layer by the interior streamfunction.

Bearing these considerations in mind, we can look again at the results presented by Cessi (1991). On a western boundary aligned with the planetary vorticity gradient (i.e. the y axis) we have $\partial\zeta/\partial x\big|_{wall} \propto \partial Q/\partial x\big|_{wall}$, so the sign of $\partial p/\partial S\big|_{wall}$ can be determined (via (3.7), substituting $-x$ for r and noting that $\tau_{||} = 0$ in this model) from the angle at which Q contours meet the western boundary. For example, in Figure 7 of Cessi (1991) there is a region of large Q against the southern part of the western boundary, which extends into the interior just upstream of the separation point. Within this separation region the pressure gradient is favorable where the Q contours emerge from the boundary in a southeasterly direction, and adverse where the Q contours emerge in a northeasterly direction (north of $Y \approx 510$ km and $Y \approx 550$ km in Cessi's Figures 7 (a) and 7 (b), respectively). Using this indicator it is clear that the separation point Y_S lies within a region of adverse pressure gradient in Cessi's Figures 7 (a) (where $Y_S = 550$ km) and 7 (b) (where $Y_S = 588$ km), despite the pressure gradient imposed by the outer flow being favorable south of $Y_Z = 632$ km in both figures. This is also the case (but somewhat harder to see) for the flows under different conditions shown in Cessi's Figures 3 and 4. The difference between the pressure gradient at the wall and that predicted from the interior streamfunction is given by Stewart's constraint (Cessi's equation (4.6)), which indicates that flow structures between the boundary layer and interior flow impose significant pressure gradients along the wall in the separation region (see Cessi's Figure 6).

REFERENCES

Agra, C. and D. Nof. 1993. Collision and separation of boundary currents. Deep-Sea Res. 1, *40,* 2259–2282.

Baines, P. G. and R. L. Hughes. 1996. Western boundary current separation: Inferences from a laboratory model. J. Phys. Oceanogr., *26,* 2576–2588.

Beardsley, R. C. 1969. A laboratory model of the wind-driven ocean circulation. J. Fluid Mech., *38,* 255–271.

——— 1972. A numerical investigation of a laboratory analogy of the wind-driven ocean circulation. In NAS Symposium on Numerical Models of Ocean Circulation, National Academy of Sciences, Durham, New Hampshire, 311.

——— 1973. A numerical model of the wind-driven ocean circulation in a circular basin. Geophys. Fluid Dyn., *4,* 211–241.

Beardsley, R. C. and K. Robbins. 1975. The 'sliced-cylinder' laboratory model of the wind-driven ocean circulation. Part 1: Steady forcing and topographic Rossby wave instability. J. Fluid Mech., *69,* 27–40.

Becker, A. and M. A. Page. 1990. Flow separation and unsteadiness in a rotating sliced cylinder. Geophys. Astrophys. Fluid Dyn., *55,* 89–115.

Berloff, P. S. and S. P. Meacham. 1997. The dynamics of an equivalent-barotropic model of the wind-driven circulation. J. Mar. Res., *55,* 407–451.

Blandford, R. R. 1971. Boundary conditions in homogeneous ocean models. Deep-Sea Res., *18,* 739–751.

Briggs, W. L. 1980. A new class of steady solutions of the barotropic vorticity equation. Dyn. Atmos. Oceans, *4,* 67–99.

Cessi, P. 1990. Recirculation and separation of boundary currents. J. Mar. Res., *48,* 1–35.

——— 1991. Laminar separation of colliding western boundary currents. J. Mar. Res., *49,* 697–717.

Cessi, P., R. V. Condie and W. R. Young. 1990. Dissipative dynamics of western boundary currents. J. Mar. Res., *48,* 677–700.

Cessi, P., G. R. Ierley and W. R. Young. 1987. A model of the inertial recirculation driven by potential vorticity anomalies. J. Phys. Oceanogr., *17,* 1640–1652.

Dengg, J. 1993. The problem of Gulf Stream separation: A barotropic approach. J. Phys. Oceanogr., *23,* 2182–2200.

Dengg, J., A. Beckmann and R. Gerdes. 1996. The Gulf Stream separation problem, *in* The Warmwatersphere of the North Atlantic Ocean, W. Krauss, ed., Gebrüder Borntraeger, Berlin, Stuttgart, 253–290.

Greenspan, H. P. 1963. A note concerning topography and inertial currents. J. Mar. Res., *21,* 147–154.

Griffiths, R. W. and A. E. Kiss. 1999. Flow regimes in a wide 'sliced-cylinder' model of homogeneous β-plane circulation. J. Fluid Mech., *399,* 205–236.

Haidvogel, D., J. McWilliams and P. Gent. 1992. Boundary current separation in a quasigeostrophic, eddy-resolving ocean circulation model. J. Phys. Oceanogr., *22,* 882–902.

Holland, W. R. and L. B. Lin. 1975. On the generation of mesoscale eddies and their contribution to the oceanic general circulation. II: A parameter study. J. Phys. Oceanogr., *5,* 658–669.

Ierley, G. R. 1987. On the onset of inertial recirculation in barotropic general circulation models. J. Phys. Oceanogr., *17,* 2366–2374.

Ierley, G. R. and O. G. Ruehr. 1986. Analytic and numerical solutions of a nonlinear boundary-layer problem. Studies in Appl. Math., *75,* 1–36.

Ierley, G. R. and V. A. Sheremet. 1995. Multiple solutions and advection-dominated flows in the wind-driven circulation. Part 1: Slip. J. Mar. Res., *53,* 703–737.

Ierley, G. R. and W. R. Young. 1988. Inertial recirculation in a β-plane corner. J. Phys. Oceanogr., *18,* 683–689.

Kamenkovich, V. M. 1966. A contribution to the theory of the inertial-viscous boundary layer in a two-dimensional model of ocean currents. Izv. Akad. Nauk. SSSR Atmos. Oceanic Phys., *2,* 781–792.

Kiss, A. E. 2000. Dynamics of laboratory models of the wind-driven ocean circulation. PhD thesis, Australian National University. Available from http://thesis.anu.edu.au/public/adt-ANU20011018.115707/index.html.

—— 2001. Potential vorticity "crises" and western boundary current separation. In 14th Australasian Fluid Mechanics Conference, B. B. Dally, ed. Adelaide University, Adelaide, Australia, pp. 901–904.

McWilliams, J. C. 1996. Modeling the oceanic general circulation. Ann. Rev. Fluid Mech., *28,* 215–248.

Moro, B. 1988. On the nonlinear Munk model, I: Steady flows. Dyn. Atmos. Oceans, *12,* 259–287.

Munk, W. H. 1950. On the wind-driven ocean circulation. J. Meteor., *7,* 79–93.

Ou, H. W. and W. P. M. de Ruijter. 1986. Separation of an inertial boundary current from a curved coastline. J. Phys. Oceanogr., *16,* 280–289.

Özgökmen, T. M., E. P. Chassignet and A. M. Paiva. 1997. Impact of wind forcing, bottom topography, and inertia on midlatitude jet separation in a quasigeostrophic model. J. Phys. Oceanogr., *27,* 2460–2476.

Page, M. A. 1982. A numerical study of detached shear layers in a rotating sliced cylinder. Geophys. Astrophys. Fluid Dyn., *22,* 51–69.

Parsons, A. T. 1969. A two-layer model of Gulf Stream separation. J. Fluid Mech., *39,* 511–528.

Pedlosky, J. 1965. A necessary condition for the existence of an inertial boundary layer in a baroclinic ocean. J. Mar. Res., *23,* 69–72.

—— 1987. Geophysical Fluid Dynamics. Springer, New York, 2nd ed.

—— 1996. Ocean Circulation Theory. Springer, Berlin, 1st ed.

Pedlosky, J. and H. P. Greenspan. 1967. A simple laboratory model for the oceanic circulation. J. Fluid Mech., *27,* 291–304.

Rhines, P. B. and R. Schopp. 1991. The wind-driven circulation: Quasi-geostrophic simulations and theory for nonsymmetric winds. J. Phys. Oceanogr., *21,* 1438–1469.

Schlichting, H. 1968. Boundary-Layer Theory. McGraw-Hill, New York, 6th ed.

Spitz, Y. H. and D. Nof. 1991. Separation of boundary currents due to bottom topography. Deep-Sea Res., *38,* 1–20.

Stommel, H. 1948. The westward intensification of wind-driven ocean currents. Trans. Am. Geophys. Union, *29,* 202–206.

Tritton, D. J. 1988. Physical fluid dynamics. Oxford Science Publications, 2nd ed.

Veronis, G. 1973. Model of world ocean circulation: I. Wind-driven, two layer. J. Mar. Res., *31,* 228–288.

Verron, J. and E. Blayo. 1996. The no-slip condition and separation of western boundary currents. J. Phys. Oceanogr., *26,* 1938–1951.

Verron, J. and J.-H. Jo. 1994. On the stability of wind-driven barotropic ocean circulations. Fluid Dyn. Res., *14,* 7–27.

Verron, J. and C. Le Provost. 1991. Response of eddy-resolved general circulation numerical models to asymmetrical wind forcing. Dyn. Atmos. Oceans, *15,* 505–533.

Received: *14 May, 2002;* revised: *18 November, 2002.*